

Article

Fabrication and Thermal Properties of Capric Acid/Calcinated Iron Tailings/Carbon Nanotubes Composite as Form-Stable Phase Change Materials for Thermal Energy Storage

Peng Liu ^{1,2,3,†}, Xiaobin Gu ^{4,†}, Zhikai Zhang ⁵, Jianping Shi ^{1,*}, Jun Rao ² and Liang Bian ² 

¹ School of Electronic & Communication Engineering, Guiyang University, Guiyang 550005, China; llp800@126.com

² School of Gemology and Materials Technology, Hebei GEO University, Shijiazhuang 050031, China; raojun@hgu.edu.cn (J.R.); bianliang@swust.edu.cn (L.B.)

³ Key Laboratory of Solid Waste Treatment and Resource Recycle, Ministry of Education, South West University of Science and Technology, Mianyang 621010, China

⁴ Materials Interfaces Center, Shenzhen Institutes of Advanced Technology, Chinese Academy of Sciences, Shenzhen 518005, China; xb.gu@siat.ac.cn

⁵ School of Water Resources and Environment, Hebei GEO University, Shijiazhuang 050031, China; zhkzhang@ipe.ac.cn

* Correspondence: sjpdxy@gyu.cn

† These co-first authors contributed equally to this work.

Received: 16 September 2019; Accepted: 15 October 2019; Published: 23 October 2019



Abstract: In this study, a novel form-stable phase change material (FSPCM) consisting of calcination iron tailings (CIT), capric acid (CA), and carbon nanotubes (CNT) was prepared using a simple direct melt impregnation method, and a series of tests have been carried out to investigate its properties. The leakage tests showed that CA can be retained in CIT with a mass fraction of about 20 wt.% without liquid leakage during the phase change process. Moreover, the morphology, chemical structure, and thermal properties of the fabricated composite samples were investigated. Scanning electron microscope (SEM) micrographs confirmed that CIT had a certain porous structure to confine CA in composites. According to the Fourier transformation infrared spectroscopy (FTIR) results, the CA/CIT/CNT FSPCM had good chemical compatibility. The melting temperature and latent heat of CA/CIT/CNT by differential scanning calorimeter (DSC) were determined as 29.70 °C and 22.69 J/g, respectively, in which the mass fraction of CIT and CNT was about 80 wt.% and 5 wt.%, respectively. The thermal gravity analysis (TGA) revealed that the CA/CIT/CNT FSPCM showed excellent thermal stability above its working temperature. Furthermore, the melting and freezing time of CA/CIT/CNT FSPCM doped with 5 wt.% CNT reduced by 42.86% and 54.55% than those of pure CA, and it showed better heat transfer efficiency. Therefore, based on the above analyses, the prepared CA/CIT/CNT FSPCM is not only a promising candidate material for the application of thermal energy storage in buildings, but it also provides a new approach for recycling utilization of iron tailings.

Keywords: capric acid; calcinated iron tailings; carbon nanotubes; FSPCM; thermal energy storage

1. Introduction

In recent years, the environmental issue and the energy crisis are driving people to develop renewable energy. However, low utilization efficiency and poor stability hinder the large-scale applications of renewable energy [1]. In addition, the sharp unbalance contradiction of energy supply and demand makes it urgent to develop energy storage technology to store the renewable energy [1,2].

Thermal energy storage (TES) as an efficient and clean method can improve energy utilization efficiency and ease the contradiction between energy supply and demand [2]. In the TES technologies, the latent heat storage using phase change materials (PCMs) was considered to be one of the promising solutions due to their many advantages such as high energy storage density, nearly constant temperature during thermal energy storage, etc. [3]. Therefore, PCMs are widely researched and applied in many fields, including air-conditioning [4,5], electronic devices [6–10], waste heat recovery [11,12], building energy [13,14], smart textile [15,16], and solar energy storage [17,18]. According to the phase change process, PCMs can be divided into solid-liquid, solid-solid, solid-gas, and liquid-gas categories [19]. Moreover, the solid-liquid PCMs can be divided into inorganic and organic ones. Presently, intensive studies have been conducted on organic PCMs, for fatty acids have many useful characteristic properties such as appropriate suitable phase change temperature, high heat latent value, almost no super-cooling, nontoxic, etc. [20,21]. Although fatty acids exhibit excellent properties, leakage issue and low thermal conductivity seriously impede their practical applications. Hence, it is very necessary to overcome the two shortcomings mentioned above.

In order to hold back the leakage of fatty acids during the working process, the syntheses of form-stable PCMs (FSPCMs) by adsorbing fatty acids into different supporting materials have been widely researched in the past few years [22]. In practice, there are two main methods to be usually used to prepare the FSPCMs: (1) Encapsulation of fatty acids into a macro or micro dimension microcapsule structure, namely, microcapsule technology [23]; (2) simply impregnated fatty acids into various porous materials. Obviously, the second one has remarkable advantages of low cost, simple operation, unique pore structure, and easily available materials [22]. As a result, different porous materials were employed to prepare FSPCMs, thereinto, clay mineral-based FSPCMs were extensively studied such as expanded graphite [24,25], perlite [26], kaolinite [27,28], diatomite [29,30], and meteorite [31]. A large number of research results demonstrated that by adsorbing PCM into porous material to fabricate FSPCMs, the liquid leakage problems can be effectively solved [32,33]. However, the fabrication of FSPCMs is relatively costly by these natural porous mineral clay materials compared with the preparation of solid waste-based FSPCM. Moreover, the reserves of natural porous mineral clay materials are exhaustible. Fortunately, iron tailings (ITs) are a kind of solid waste produced from iron ore separation, and they are very cheap and quite easily available. Meanwhile, the treatment and recycling utilization of iron tailings have always been a problem. The comprehensive utilization is becoming one of the hot social topics all over the world [34–37]. It is worth noting that the main chemical components of typical iron tailings are similar to several natural mineral materials reported in the literature [38]. The chemical components such as SiO_2 , Al_2O_3 , and MgO can be used as porous materials. Moreover, some of the chemical components in IT such as Na_2O and K_2O have a fluxing effect, which make ITs possible to be used as a supporting material of PCM. Therefore, the iron tailings were calcinated to prepare porous mineral materials in this study.

To overcome poor thermal conductivity of fatty acids, a lot of efforts have been made to synthesize composite PCMs by adding additives with high thermal conductivity. The introduction of thermal conductivity enhancers has been proven to be a superior way to effectively improve the thermal conductivity of fatty acids. Therefore, many researchers attempt to add thermal conductivity enhancers into PCMs, mainly including carbon nanofibers (CNF) [39], activated carbon (AC) [40], expanded graphite (EG) [41], graphene [42], and carbon nanotubes (CNT) [43,44]. Among the investigated thermal conductivity enhancers, CNT was considered to be a promising enhancer of thermal conductivity in future practical applications and has been a research hotspot in recent years. The feasibility and effectiveness have also been verified by the above-mentioned literatures [43,44]. Therefore, CNT was employed to be as the thermal conductivity enhancer in this work.

This study aims to fabricate an FSPCM with an appropriate phase change temperature, good thermal conductivity, and high heat latent, which could be used in the intelligent temperature control of buildings. In the FSPCM composite, capric acid (CA) is one of the promising fatty acids used for building energy conservation because of its suitable phase change temperature and high phase

change latent heat. Particularly, the phase change temperature of CA is within the human body comfortable temperatures. Hence, CA was chosen as the PCM in this research. Considering the cost, simple preparation, and practical utility, the iron tailings were pretreated firstly by calcination. Then, the obtained calcination iron tailings (CIT) were acted as the supporting material to prevent the liquid CA leakage. Additionally, CNT was used as the thermal conductivity enhancer to improve the thermal conductivity of CA. The composite PCMs were prepared through the facile direct impregnation method. The prepared CA/CIT/CNT FSPCM has great potential for TES application in buildings. Simultaneously, it creates an innovative approach for recycling utilization of iron tailings.

2. Experiment

2.1. Material

The CA was purchased from Sinopharm Chemical Reagent Co., Ltd. (Shanghai, China). The iron tailings were obtained from the Hanxing Mining Bureau (Handan, China). The iron tailings were firstly screened into -60 mesh. Additionally, the sample was mixed with a montmorillonite binder additive (provided from Yipusheng Tianjin Pharmaceutical Co., Ltd.). Then, the mixture was roasted in a high-frequency furnace at about 300 °C for 30 min. After that, the mixture was heated at 600 °C for 120 min. The cooled residual ash sample became CIT to package PCM. As seen from Table 1, CIT has similar chemical components as some typical minerals and this indicates that it can be used as carrier matrix to prepare mineral-based composite phase change materials in theory. The CNT was supplied by Suzhou Tanfeng Tech, Inc. (Suzhou, China). The main properties of the CA and CNT were given in Table 2.

Table 1. Comparison of chemical constituent of iron tailings, calcination iron tailings (CIT), and some typical natural minerals [45,46].

Material	SiO ₂	Al ₂ O ₃	Fe ₂ O ₃	CaO	MgO	K ₂ O + Na ₂ O	Others
Iron tailings	31.98	6.49	10.23	30.77	13.84	1.64	5.05
CIT	33.97	7.23	10.59	31.14	13.91	1.66	1.50
Diatomite	97.91	1.04	0.65	-	0.05	0.12	0.23
Perlite	74.6	13.1	0.83	0.83	0.19	7.87	2.58

Table 2. Main properties of capric acid (CA) and carbon nanotubes (CNT).

Properties	CA	CNT
CAS number	334-48-5	308068-56-6
Chemical formula	C ₁₀ H ₂₀ O ₂	-
Molecular weight	172.26	-
Purity (%)	98.5	91%
Melting point (°C)	31.4 °C	3550 °C
Solidifying point (°C)	≥29.0 °C	-
Thermal conductivity (w/(m·k))	-	2860

2.2. Preparation of FSPCM

As shown in Figure 1, the FSPCM was fabricated according to the following two steps. First of all, the different mass ratio of CA and CIT were put into different beakers and evenly mixed, respectively. Then, the mixtures were heated and evenly stirred on the water bath at 60 °C for 30 min. After they were cooled down to room temperature for 2 h, the composites were formed. Then, the leakage tests were carried out through the simple and effective method reported by the literature 47–50 [47–50]. Secondly, the CA/CIT sample without leakage and maximum adsorption capacity of CA was mixed with 1 wt.%, 3 wt.%, 3 wt.%, and 7 wt.% CNT in 25 mL beakers, respectively. Moreover, the preparation procedures of the sample composites in the first step were repeated. Thus, the CA/CIT/CNT FSPCMs can be obtained.

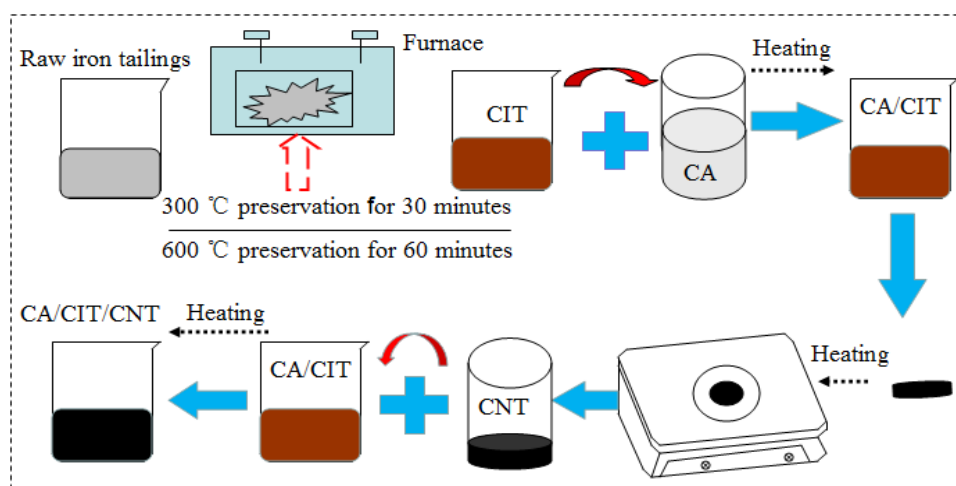


Figure 1. Preparation process of CA/CIT/CNT composites.

2.3. Characterization of FSPCM

The leakage tests were conducted on the constant magnetic stirrer by taking advantage of the diffusion-oozing testing method. Before testing, 3 g CA/CIT composites consisting of different mass fractions of CA and CIT were separately pressed at 12 MPa for 3 min in the mould with the diameter of 3 cm. The made-up samples similar to small round flakes were put on the medium speed filter papers, respectively. Then, the samples along with the corresponding filter paper were placed in the constant humidity magnetic stirrer to be heated at 60 °C for 10 min. The leakage phenomenon and the result of the samples can be observed during the heating process. The leakage stain of every sample was measured by a ruler with a test error of ± 0.5 mm. The amounts of the samples were weighed by digital electronic precision balance with one-thousandth precision. The microstructure of CA, CIT, CNT, CA/CIT, and CA/CIT/CNT FSPCM were characterized by scanning electron microscope (SEM). The chemical characterization of the constituents of FSPCM was evaluated by using Fourier transformation infrared spectroscopy (FTIR) at a wavenumber range of 400–4000 cm^{-1} . The melting temperature and latent heat of CA/CIT and CA/CIT/CNT FSPCM were measured by differential scanning calorimeter (DSC) at the heating/cooling rate of 10 °C/min under N_2 gas atmosphere. The thermal gravity analyses (TGA, from 20–600 °C) of CA, CA/CIT, and CA/CIT/CNT were used to investigate the thermal stability of FSPCM. The thermal storage and release performance were conducted by using an intelligent paperless recorder. For this purpose, the same amount of CA, CA/CIT FSPCM, and CA/CIT/CNT FSPCM were put into centrifuge tubes, respectively. Then, the thermocouple was embedded into the centrifuge tube, while the other was connected to the intelligent paperless recorder. After that, all the centrifuge tubes were placed into the refrigerator at -10 °C to maintain the same starting temperature. When the experiments were started, they were placed into the water bath at room temperature. The temperature range of the sample was -10 to 60 °C for the heating process, while 60 to -10 °C for the freezing process, respectively. When the temperature of the water bath rose up to 60 °C, it was kept for half an hour during the heating process. The temperature data during the whole process of heat storage/release were continuously recorded by the intelligent paperless recorder.

3. Results and Discussion

3.1. The Leakage Tests of CA/CIT/CNT Composites

The sample tablets of CA/CIT composites used in the leakage tests were given in Figure 2. The testing results were shown in Figure 3. Obviously, the leakage is more and more serious from Figure 3d to Figure 3a, while the leakage of CA liquid cannot be observed in Figure 3e,f. Usually, no leakage of PCM is the basic criterion to evaluate the package efficiency of FSPCM. Hence, the sample

S1-5 can be considered to be the FSPCM without liquid leakage. Sometimes, the sample without any liquid stains of CA on filter paper after heating can also be used to evaluate the package efficiency of FSPCM. Therefore, the liquid stains of CA in CA/CIT on the filter paper were furthermore shown in Figure 4. As seen from Figure 4, sample S1-6 indicates no liquid leakage formed in the FSPCM while there was a small liquid stain of the sample S1-5 on the filter paper. To quantify the leakage of CA, the leakage ratio was introduced, which is the weight of leaked CA divided by the total weight of CA in the corresponding composites [32]. As seen in Table 3, the leakage ratios of S1-5 and S1-6 were quite smaller than the others so that their leakage could be negligible. Furthermore, the CNT can also be employed to act as the supporting material. When CNT was added into the CA/CIT FSPCM, the leakage ratio of FSPCM would be much lower than without CNT at the mass fraction of S1-5. Therefore, to be a comprehensive consideration, the sample S1-5 in the first step can be considered to be the FSPCM used in the second step. In the same way, when the CA/CIT FSPCM was fabricated by mixing the specified amount of CNT during the second step, the thermal conductivity enhancer CNT was added into the CA/CIT FSPCM to fabricate CA/CIT/FSPCM.

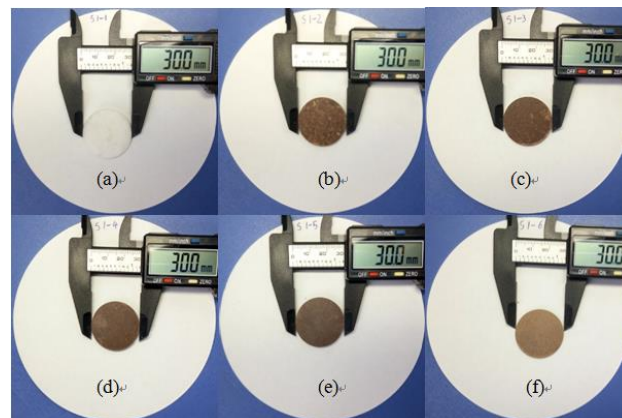


Figure 2. Sample tablets of CA/CIT composites used in leakage tests. (a) S1-1, (b) S1-2, (c) S1-3, (d) S1-4, (e) S1-5, (f) S1-6.

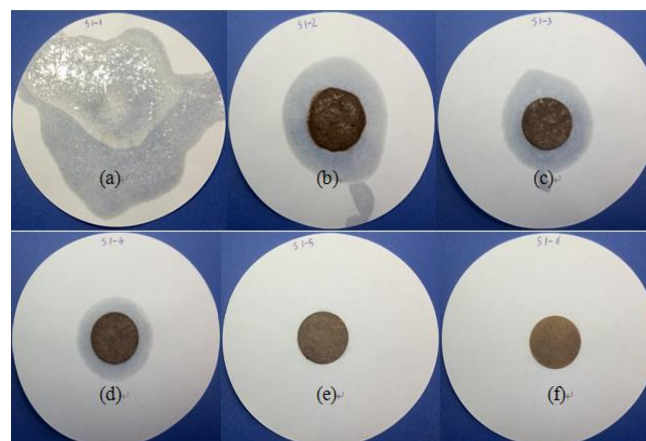


Figure 3. Leakage test results obtained at 60 °C of CA/CIT composites. (a) S1-1, (b) S1-2, (c) S1-3, (d) S1-4, (e) S1-5, (f) S1-6.

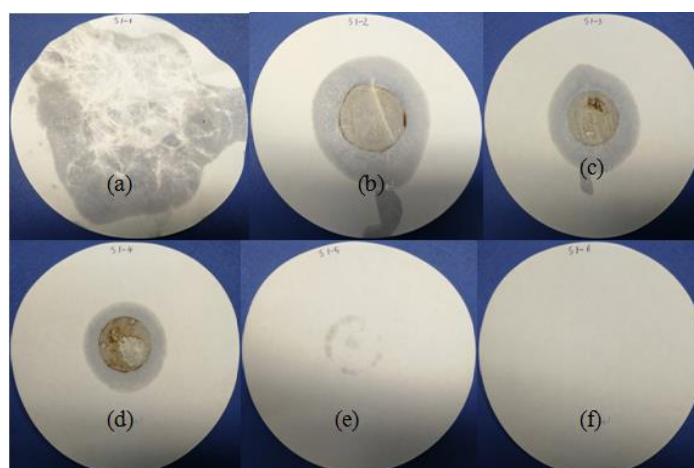


Figure 4. Liquid stains of CA in CA/CIT composites on the filter paper after heating at 60 °C. (a) S1-1, (b) S1-2, (c) S1-3, (d) S1-4, (e) S1-5, (f) S1-6.

Table 3. Basic proportion and leakage results of CA/CIT composites.

Step	Sample	The Composition Ratio of the CA/CIT Composites	Leakage Ratio (%)	Leakage Area of the Sample (cm ²)
1	S1-1	Pure CA	46.07	72.35
1	S1-2	50% CA + 50% CIT	21.80	39.57
1	S1-3	40% CA + 60% CIT	15.43	26.41
1	S1-4	30% CA + 70% CIT	12.89	18.85
1	S1-5	20% CA + 80% CIT	0.50 (negligible)	(Missing)
1	S1-6	10% CA + 90% CIT	0.33 (negligible)	0

To quantitatively evaluate the leakage results, the leakage area and leakage ratios of CA/CIT composites were calculated and shown in Figures 5 and 6. From Figures 5 and 6, it can be clearly seen that both the leakage area and the leakage ratio of CA/CIT composites increase monotonously with the increasing of the mass fraction of CIT. Moreover, the linear relationships can be described as the following formulations, respectively.

$$Y_1 = -0.5931X_1 + 48.8259, R^2 = 0.9773$$

where Y_1 represents the leakage ratio of sample, %. X_1 represents the mass fraction of sample, %.

$$Y_2 = -0.9539X_2 + 73.9642, R^2 = 0.9757$$

where Y_2 represents the leakage area of sample, cm². X_2 represents the mass fraction of sample, %.

Obviously, when the mass fraction of CIT is about 80%, the leakage area and the leakage ratio of CA/CIT composites are very small and negligible. Furthermore, the mentioned relationships may provide a relatively feasible quantitative method to evaluate and judge the leakage of PCM composites.

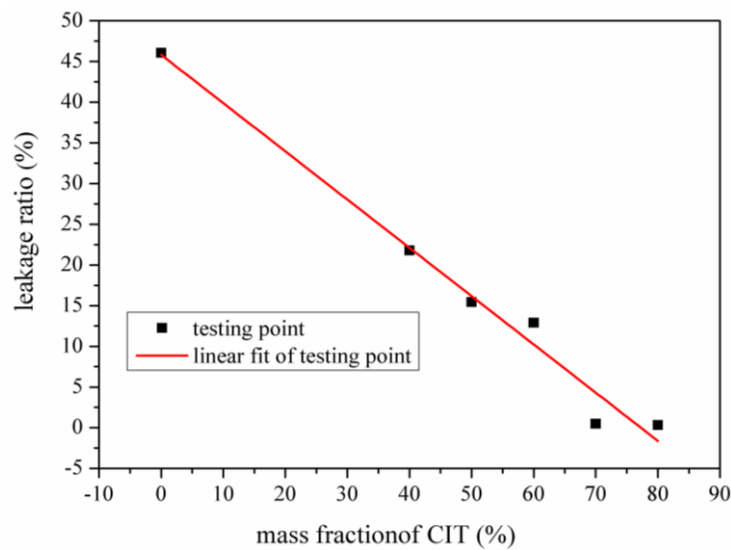


Figure 5. Leakage area of CA/CIT composites with different mass fractions of CIT.

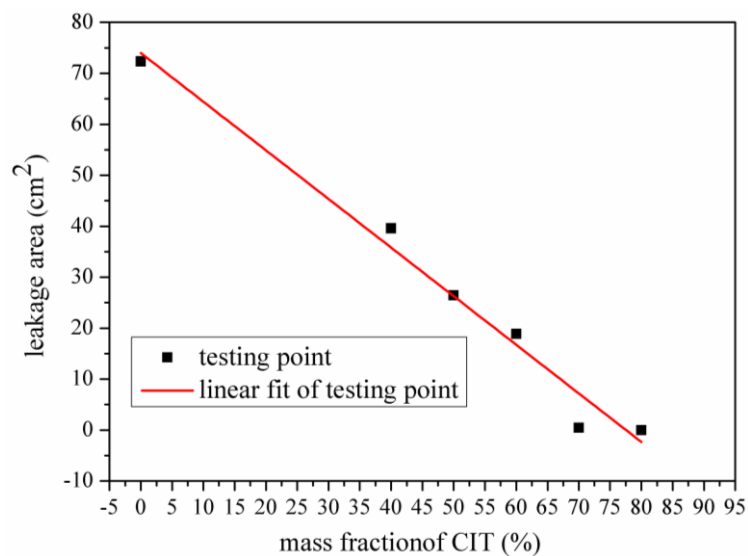


Figure 6. Leakage ratios of CA/CIT composites with different mass fractions of CIT.

3.2. Morphology of the CA, CIT, CNT, CA/CIT, and CA/CIT/CNT Composites

Figure 7 shows the SEM images of CA, CIT, CA/CIT FSPCM, and CA/CIT/CNT FSPCM. As shown in Figure 7a, the CA displayed the viscous paste liquid. From Figure 7b, it can be seen that the CIT had a porous microstructure. As seen from Figure 7c, the CNT looked like an expanded cotton fluff with various pore network structures. As observed from Figure 7d, the surface of CIT was covered by the impregnated CA. Simultaneously, most of the porous hole of CIT were completely covered and the porous holes were reduced. This indicated that the suitable amount of CA could be absorbed into porous holes of CIT due to capillary and surface tension forces among the components. As clearly noticed from Figure 7e,f, some CNT was covered on the surface porous hole of CIT, which confirmed that the CNT was successfully impregnated into the synthesized FSPCM, while most of the CNT was filled into CIT particles. This is the reason why CNT can enhance the heat transfer efficiency of CA by constructing path channels for CA successfully.

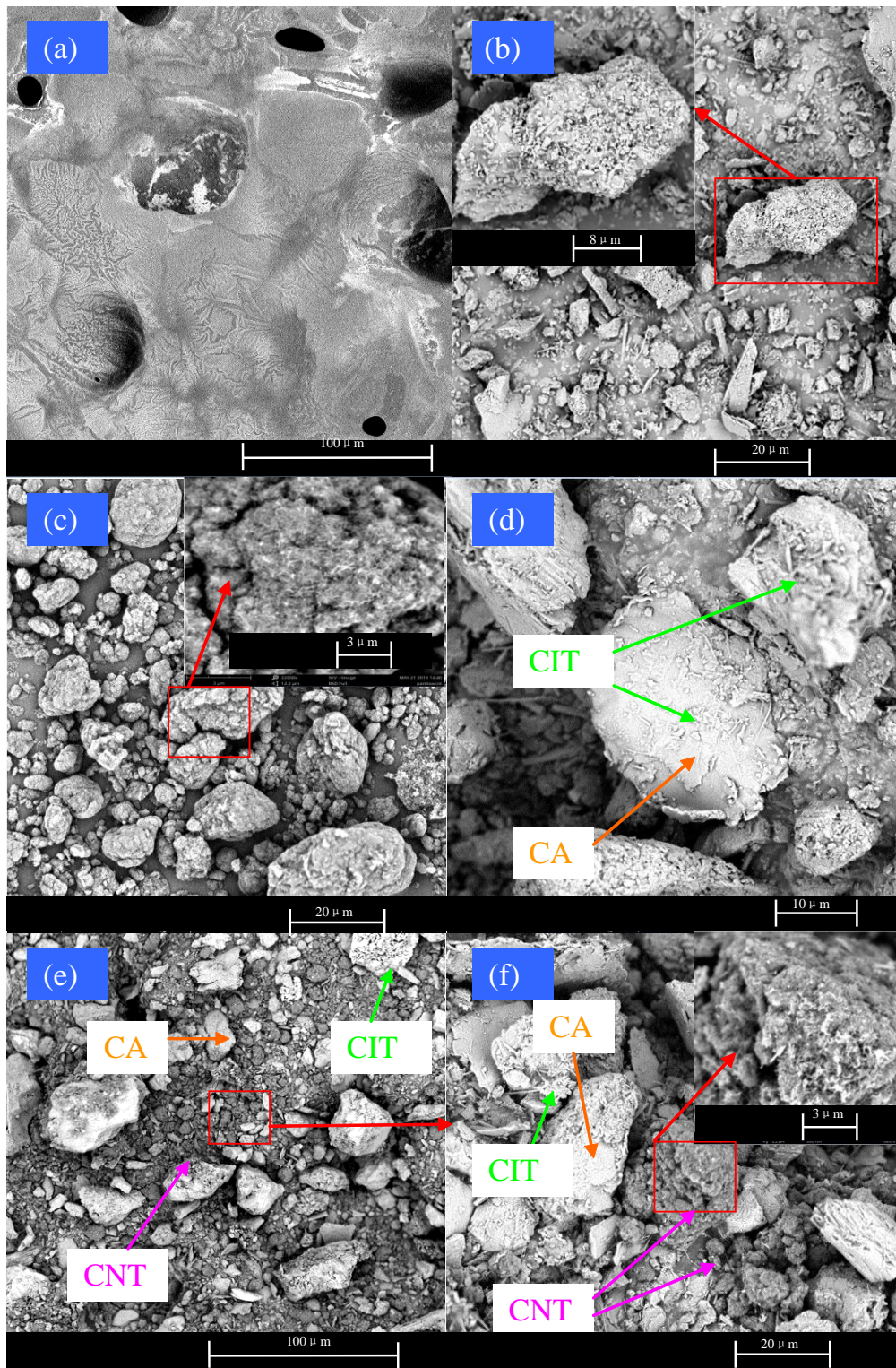


Figure 7. SEM photographs of CA (a), CIT (b), CNT (c), CA/CIT (d), CA/CIT/CNT, (e) and (f).

3.3. Chemical Compatibility of the CA/CIT/CNT Composites

The FTIR spectrums of the CA, CIT, CA/CIT FSPCM, and CA/CIT/CNT FSPCM were given in Figure 8. It can be seen that in the spectrum of pure CA, the absorption peaks at 939, 1410, and 1710 cm^{-1} corresponded to the stretching vibrations of $-\text{OH}$, $\text{C}=\text{O}$, and COO^- , respectively. The characteristic peaks at 2850 and 2930 cm^{-1} represented symmetric stretching vibrations of $-\text{CH}_3$

and $-\text{CH}_2$, respectively [51,52]. In the spectrum of CIT, the bands at 476, 695, and 882 cm^{-1} can be ascribed to the stretching of the Si–O–Si group. Additionally, the stretching vibrations of the Si–O group appeared in 1090 and 1170 cm^{-1} . The spectrums of CA/CIT and CA/CIT/CNT showed the primary peaks of CA and CIT, and CNT had no effect on the spectrum peaks of composites. Moreover, no other additional peaks occurred in the fabricated FSPCMs except for slight changes in the intensity of some peaks because of weak physical interaction such as, hydrogen bonding interactions, surface tension force, and capillary force. These findings indicated that there was only physical interaction among CA, CIT, and CNT in composites without any kind of chemical action. Hence, FTIR results confirmed that FSPCM had good chemical compatibility among the constituents in FSPCM. Moreover, the physical interaction largely contributed to the shape-stabilization of CA/CIT because the CA molecules were firmly tied to CIT pores by the confinement effect.

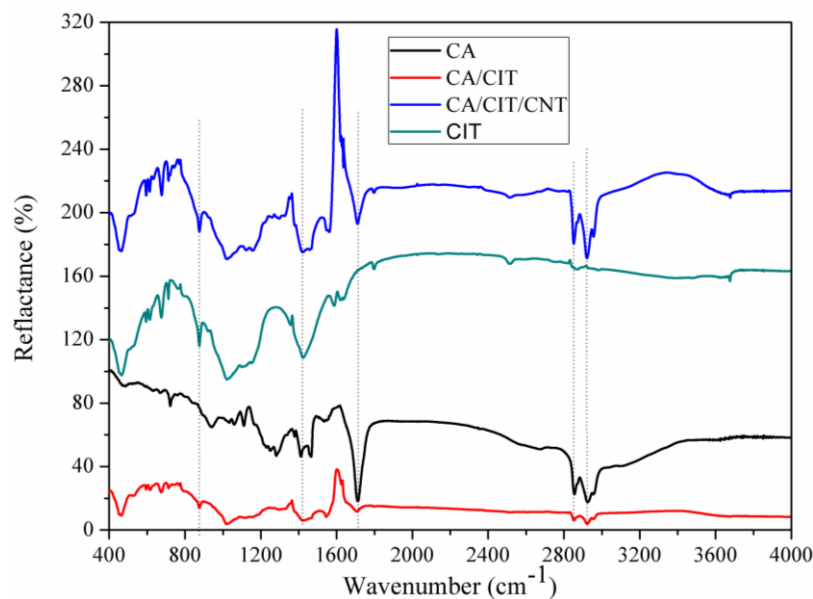


Figure 8. FTIR spectra of CA, CIT, CA/CIT, and CA/CIT/CNT samples.

3.4. Thermal Properties of the CA/CIT/CNT FSPCMs

The thermal properties including latent heat value and phase change temperature of CA/CIT FSPCM and CA/CIT/CNT FSPCM were examined by DSC. The DSC curves and data of CA/CIT FSPCM and CA/CIT/CNT FSPCM are shown in Figure 9 and Table 4. As seen from Figure 9 and Table 4, the melting temperature and freezing temperature of CA/CIT FSPCM and CA/CIT/CNT FSPCM were determined as 35.89 and 26.8 °C for CA, as 30.73 and 26.77 °C for CA/CIT FSPCM, as 29.70 and 26.09 °C for CA/CIT/CNT FSPCM, respectively. In comparison with pure CA, the melting temperatures of the composites were diminished by 5.16 and 6.19 °C, respectively. Compared to pure CA, the freezing temperatures of composites were reduced by 0.03 and 0.71 °C, respectively. In addition, there was a difference between the freezing temperature and melting temperature. The reason may be the physical interaction among the components in composites. Fortunately, the phase change temperature of composites is closed to the comfortable room temperature of 20–26 °C, so the prepared CA/CIT FSPCM is suitable for application in buildings. Moreover, the thermal enthalpy of CA, CA/CIT FSPCM, and CA/CIT/CNT FSPCM are 169.5, 25.14, and 22.69 J/g during the melting process, respectively. The comparisons of thermal properties between this work and some other literatures were also listed in Table 4. Although the thermal enthalpy of CA/CIT/CNT FSPCM is slightly lower than that of some literatures, it has many advantages over other materials in building applications such as low cost, wide source, large in quantity, easy to use, and simple process. In short, we can conclude that the fabricated CA/CIT/CNT FSPCM has TES potential in buildings as energy-saving materials.

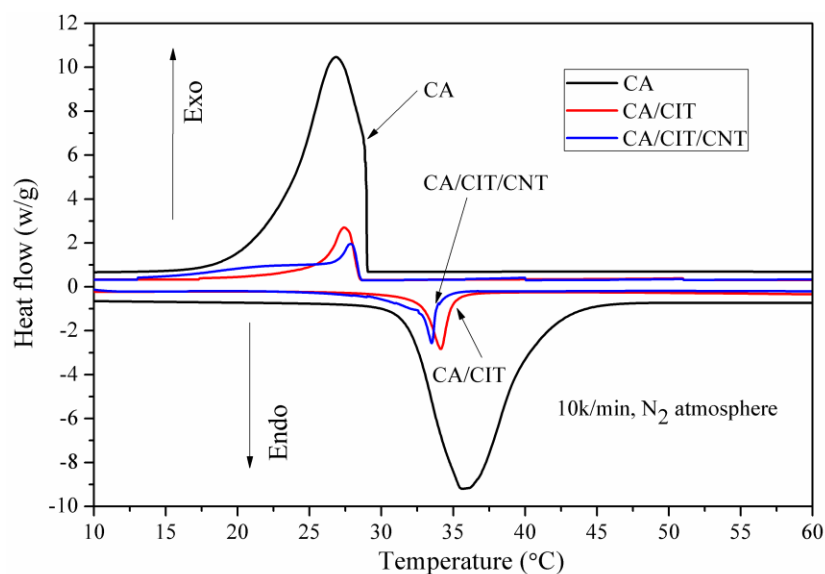


Figure 9. DSC curves of CA, CA/CIT form-stable phase change material (FSPCM), and CA/CIT/CNT FSPCM.

Table 4. Thermal properties and results comparison with some literatures.

Item	Melting Temperature (°C)	Solidifying Temperature (°C)	Latent Heat of Melting (J/g)	Latent Heat of Solidifying (J/g)	References
Capric-myristic acid (20 wt.)/VMT	19.8	17.1	27.46	31.42	[53]
Capric-myristic acid (20 wt.)/VMT + EG (2 wt.%)	19.7	17.1	26.9	(Missing)	[53]
Capric-lauric acid (26 wt.)/gypsum	19.11	(Missing)	35.24	(Missing)	[54]
Dodecanol (25–30 wt.)/gypsum	20.0	21.0	17.0	(Missing)	[55,56]
Propyl palmitate (25–30 wt.)/gypsun	19.0	16.0	40.0		[55,56]
Capric-lauric acid (25–30 wt.%) + fire retardant/gypsum	17.0	21.0	28.0	(Missing)	[57]
Paraffin (18 wt.)/kaolin	23.9	26.3	27.9	(Missing)	[58]
Xylitol pentalaurate (19 wt.)/cement	44.07	41.08	31.09	27.36	[59]
Xylitol pentalaurate (20 wt.)/gypsum	40.44	39.53	31.77	29.47	[59]
Capric-palmitic acid (25 wt.)/gypsum wallboard	21.12	21.46	36.23	38.28	[60]
Emerest 2326 (25.7 wt.)/gypsum	16.32	19.7	34.77	33.97	[61]
PA (25 wt.)/active aluminum oxide	74.13	59.57	28.56	17.53	[62]
S1-5 (CA 20 wt.% + CIT 80 wt.%)	30.73	28.98	25.14	23.05	This study
CA/CIT/CNT (CA20 wt.% + CIT 80 wt.)/CNT 5 wt.%)	29.70	28.09	22.69	21.17	This study

3.5. Thermal Stability of the CA/CIT/CNT FSPCMs

The thermal stability of CA, CA/CIT FSPCM, and CA/CIT/CNT FSPCM were examined by TGA, and the TGA curves were presented in Figure 10. As seen from Figure 10, the weight loss percentage of CA, CA/CIT FSPCM, and CA/CIT/CNT FSPCM were 99.92%, 20%, and 18.90%, respectively. The results indicated that the mass fractions of CA confined into CIT and CIT/CNT were 20% and 18.90%, respectively. In addition, CIT was still thermally stable over 440 °C. It demonstrated that the CIT was quite feasible to act as supporting material of CA PCM. Moreover, the onset degradation temperatures of CA, CA/CIT FSPCM, and CA/CIT/CNT FSPCM were 220 °C, 380 °C, and 440 °C, respectively. The temperature limit for thermal degradation of CA/CIT FSPCM and CA/CIT/CNT was much higher than that of the working temperatures (16–26 °C). These results confirm that the CA/CIT FSPCM and

CA/CIT/CNT FSPCM have good thermal stability, which makes them more suitable for TES application in buildings.

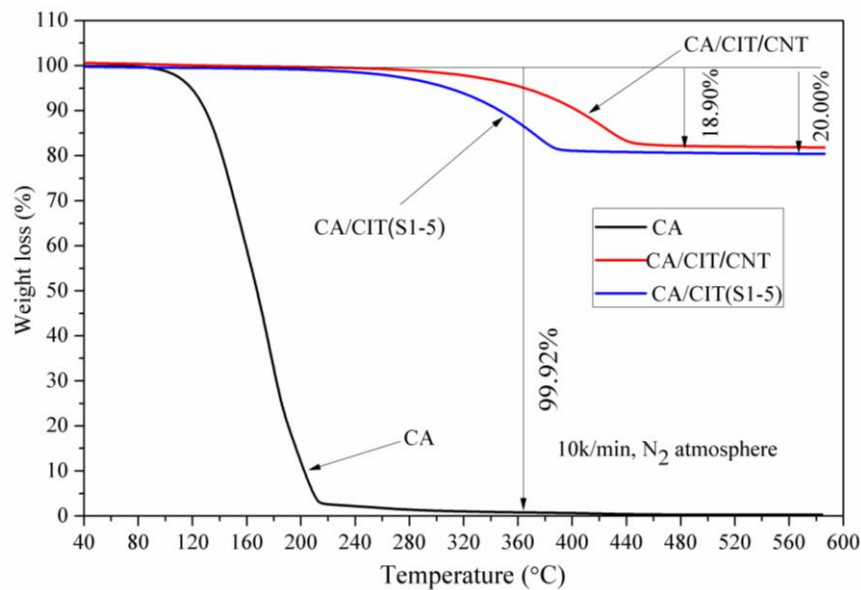


Figure 10. TGA curves of CA, CA/CIT FSPCM, and CA/CIT/CNT FSPCM.

3.6. Thermal Storage/Release Performance of the CA/CIT/CNT FSPCMs

To further evaluate the improvement efficiency of heat transfer, the thermal storage/release performance was also examined through the cooling curve method. The test method and storage efficiency definition of the melting and cooling curve in this study was the same as the condition in our previous work [63]. Moreover, the evaluation method of heat transfer of the prepared FSPCMs was also as the conditions in our previous work [63]. The melting and cooling curves of CA, CA/CIT FSPCM, and CA/CIT/CNT FSPCM with different mass fraction CNT were shown in Figure 11. From the curves of Figure 11, for a 40 °C increase in temperature (from −12 to 30 °C) during the melting process, the required time was about 21, 18, 15, 13, 12, and 11 min for CA, CA/CIT FSPCM, and CA/CIT/CNT FSPCM, respectively. Compared with the melting time of CA and CA/CIT FSPCM, the melting time was reduced by 47.62% and 38.89%, respectively for CA/CIT/CNT (7 wt.%) whereas it was reduced by 42.86% and 33.33% for CA/CIT/CNT (5 wt.%). In a similar way, for a 40 °C decrease in temperature (from 30 to −12 °C) during the solidifying process, the passed time was about 22, 20, 13, 12, 10, and 8 min, respectively, for CA, CA/CIT FSPCM, and CA/CIT/CNT FSPCMs. In comparison with the freezing time of CA and CA/CIT FSPCM, it was reduced by 63.64% and 60.00%, respectively for CA/CIT/CNT (7 wt.%) whereas it was reduced by 54.55% and 50.00% for CA/CIT/CNT (5 wt.%). Moreover, the time of maintaining an equilibrium temperature platform for CA, CA/CIT FSPCM, and CA/CIT/CNT FSPCMs with different mass fractions CNT in the melting process was 12, 9, 5, 2.5, 2, and 1.8 min, respectively. Additionally, the time of maintaining the equilibrium temperature platform for CA, CA/CIT FSPCM, and CA/CIT/CNT FSPCMs during the freezing process was 14, 7, 4, 2.5, 2, and 1.8 min, respectively. The time of maintaining the equilibrium temperature platform of CA/CIT/CNT FSPCMs was less than that of CA and CA/CIT FSPCM during the melting or freezing process. The CA/CIT/CNT FSPCM exhibits a greater heat storage/release rate than CA/CIT and pure CA. These results mean that the CNT additive in FSPCM can evidently reduce the thermal storage/release time and improve heat transfer efficiency.

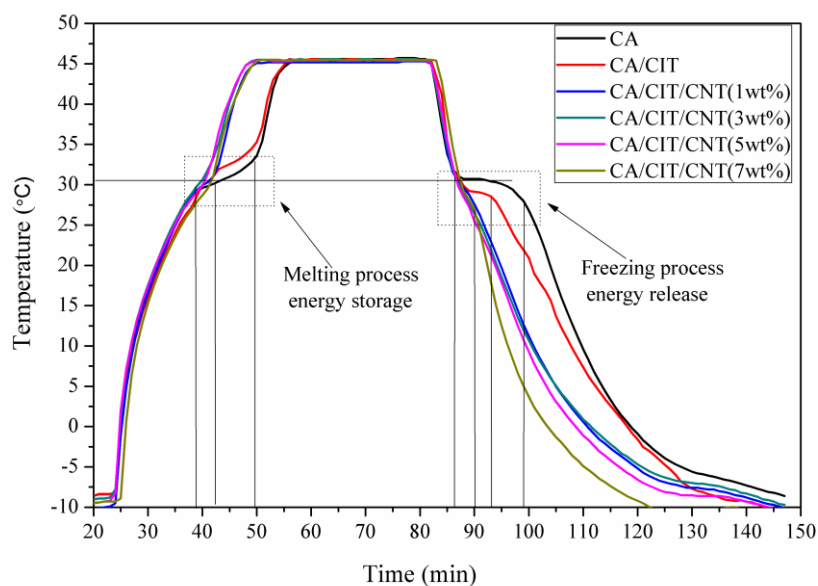


Figure 11. Storage and release curves of CA, CA/CIT FSPCM, and CA/CIT/CNT FSPCM.

4. Conclusions

In this study, CIT was used as the supporting material to prevent the liquid leakage of CA and fabricate the FSPCM. A novel CA/CIT/CNT FSPCM was developed to be used in a building TES by a facile direct impregnation method. The leakage tests reveal that both the leakage area and the leakage ratio of CA/CIT composites decrease monotonously with the increase of the mass fraction of CIT ($Y_1 = -0.5931X_1 + 48.8259$, $R^2 = 0.9773$. $Y_2 = -0.9539X_2 + 73.9642$, $R^2 = 0.9757$). The absorption of CA in CIT is about 20 wt.% without liquid leakage. The good chemical compatibility among CA, CIT, and CNT were confirmed by SEM and FTIR tests. When the mass fraction of CIT is about 80 wt.% in CA/CIT/CNT FSPCM including 5 wt.% CNT, the DSC results indicate that the fabricated CA/CIT/CNT FSPCM melts at 29.70 °C with a latent heat of 22.69 J/g and solidifies at 28.09 °C with the enthalpy of 21.17 J/g, respectively. The fabricated CA/CIT/CNT FSPCM has a suitable phase change temperature, which is close to the suitable room temperature range of 20–26 °C. The TGA analysis confirms that the CA/CIT/CNT FSPCM has good thermal stability above its working temperature. Moreover, the melting and solidifying time of the prepared CA/CIT/CNT (5 wt.%) FSPCM are 42.86% and 54.55% less than those of pure CA, respectively. The introduction of CNT can increase the thermal conductivity of CA/CIT composites and improve the storage/release performance of CA/CIT and pure CA. In conclusion, the produced CA/CIT/CNT FSPCM presents a potential choice for TES in buildings as ingredients material. Moreover, it may provide a novel path for recycling utilization of iron tailings.

Author Contributions: Conceptualization, P.L. and X.G.; methodology, P.L. and X.G.; literature review, P.L. and X.G.; investigation, P.L. and X.G.; Resources: J.R., and Z.Z.; writing—original draft preparation, P.L. and X.G.; writing—review and editing, P.L. and X.G. and Z.Z.; supervision, L.B. and J.S.; project administration, L.B. and J.S.; Funding Acquisition: J.S.

Funding: This work was financially supported by the special funding of Guiyang science and technology bureau and Guiyang University (GYU-KYZ(2019~2020)DT-13), the National Natural Science Foundation of China (41872039), the Opening Project of Key Laboratory of Solid Waste Treatment and Resource Recycle, Ministry of Education (18zxk03), Hebei Key Technology R&D Program of the Agency of Hebei province (17214016), Science and technology research Youth Fund Project of Hebei Province Higher Education (QN2018124), and Hebei Province Natural Science Foundation Youth Fund (E2019403135).

Acknowledgments: The authors would like to express their gratitude to the Instrument Chemical Analysis Center of Peking University (Beijing, China) for thermal properties analysis. Hebei GEO University Gemsbase is also warmly acknowledged for FTIR analysis.

Conflicts of Interest: The authors declare no conflict of interest.

References

1. Li, M.; Mu, B. Effect of different dimensional carbon materials on the properties and application of phase change materials: A review. *Appl. Energy* **2019**, *242*, 695–715. [[CrossRef](#)]
2. Sharma, R.K.; Ganesan, P.; Tyagi, V.V.; Metselaar, H.S.C.; Sandaran, S.C. Developments in organic solid–liquid phase change materials and their applications in thermal energy storage. *Energy Convers. Manag.* **2015**, *95*, 193–228. [[CrossRef](#)]
3. Su, X.; Jia, S.; Lv, G.; Yu, D. A unique strategy for polyethylene glycol/hybrid carbon foam phase change materials: Morphologies, thermal properties, and energy storage behavior. *Materials* **2018**, *11*, 2011. [[CrossRef](#)]
4. Said, M.A.; Hamdy, H. Effect of using nanoparticles on the performance of thermal energy storage of phase change material coupled with air-conditioning unit. *Energy Convers. Manag.* **2018**, *171*, 903–916. [[CrossRef](#)]
5. Irsyad, M.; Suwono, A.; Indartono, Y.S.; Pasek, A.D.; Pradipta, M.A. Phase change materials development from salt hydrate for application as secondary refrigerant in air-conditioning systems. *Sci. Technol. Built Environ.* **2017**, *24*, 90–96. [[CrossRef](#)]
6. Arshad, A.; Ali, H.M.; Ali, M.; Manzur, S. Thermal performance of phase change material (PCM) based pin-finned heat sinks for electronics devices: Effect of pin thickness and PCM volume fraction. *Appl. Therm. Eng.* **2017**, *112*, 143–155. [[CrossRef](#)]
7. Liang, Z.; Xing, Y.; Wang, Z.; Xin, L. The passive thermal management system for electronic device using low-melting-point alloy as phase change material. *Appl. Therm. Eng.* **2017**, *125*, 317–327.
8. Bakan, G.; Gerislioglu, B.; Dirisaglik, F.; Jurado, Z.; Sullivan, L.; Dana, A.; Lam, C.; Gokirmak, A.; Silva, H. Extracting the temperature distribution on a phase-change memory cell during crystallization. *J. Appl. Phys.* **2016**, *120*, 164504. [[CrossRef](#)]
9. Gerislioglu, B.; Ahmadvand, A.; Karabiyik, M.; Sinha, R.; Pala, N. VO₂-based reconfigurable antenna platform with addressable microheater matrix. *Adv. Electron. Mater.* **2017**, *3*, 1700170. [[CrossRef](#)]
10. Michel, A.K.U.; Chigrin, D.N.; Mass, T.W.; Schoenauer, K.; Salinga, M.; Wuttig, M.; Taubner, T. Using low-loss phase-change materials for mid-infrared antenna resonance tuning. *Nano Lett.* **2013**, *13*, 3470–3475. [[CrossRef](#)]
11. Xu, H.; Romagnoli, A.; Jia, Y.S.; Py, X. Application of material assessment methodology in latent heat thermal energy storage for waste heat recovery. *Appl. Energy* **2017**, *187*, 281–290. [[CrossRef](#)]
12. Dal Magro, F.; Xu, H.; Nardin, G.; Romagnoli, A. Application of high temperature phase change materials for improved efficiency in waste-to-energy plants. *Waste Manag.* **2018**, *73*, 322–331. [[CrossRef](#)] [[PubMed](#)]
13. Tong, X.; Xiong, X. A parametric investigation on energy-saving effect of solar building based on double phase change material layer wallboard. *Int. J. Photoenergy* **2018**, *2018*, 1–8. [[CrossRef](#)]
14. Aketouane, Z.; Malha, M.; Bruneau, D.; Bah, A.; Michel, B.; Asbik, M.; Ansari, O. Energy savings potential by integrating phase change material into hollow bricks: The case of moroccan buildings. *Build. Simul.* **2018**, *11*, 1109–1122. [[CrossRef](#)]
15. Yi, S.; Sun, S.; Deng, Y.; Feng, S. Preparation of composite thermochromic and phase-change materials by the sol–gel method and its application in textiles. *J. Text. Inst.* **2014**, *106*, 1071–1077. [[CrossRef](#)]
16. Iqbal, K.; Khan, A.; Sun, D.; Ashraf, M.; Rehman, A.; Safdar, F.; Basit, A.; Maqsood, H. Phase change materials, their synthesis and application in textiles—A review. *J. Text. Inst.* **2019**, *110*, 625–638. [[CrossRef](#)]
17. Reyes, A.; Vásquez, J.; Pailahueque, N.; Mahn, A. Effect of drying using solar energy and phase change material on kiwifruit properties. *Dry. Technol.* **2018**, *37*, 232–244. [[CrossRef](#)]
18. Liu, Z.; Chen, Z.; Fei, Y. Microencapsulated phase change material modified by graphene oxide with different degrees of oxidation for solar energy storage. *Sol. Energy Mater. Sol. Cells* **2018**, *174*, 453–459. [[CrossRef](#)]
19. Bicer, A.; Sari, A. Synthesis and thermal energy storage properties of xylitol pentastearate and xylitol pentapalmitate as novel solid-liquid PCMs. *Sol. Energy Mater. Sol. Cells* **2012**, *102*, 125–130. [[CrossRef](#)]
20. Karaipekli, A.; BicEr, A.; Sari, A.; Tyagi, V. Thermal characteristics of expanded perlite/paraffin composite phase change material with enhanced thermal conductivity using carbon nanotubes. *Energy Convers. Manag.* **2017**, *134*, 373–381. [[CrossRef](#)]

21. Zhang, H.; Gao, X.; Chen, C.; Xu, T.; Fang, Y.; Zhang, Z. A capric–palmitic–stearic acid ternary eutectic mixture/expanded graphite composite phase change material for thermal energy storage. *Compos. Part A Appl. Sci. Manuf.* **2016**, *87*, 138–145. [[CrossRef](#)]
22. Ates, M.; Caliskan, S.; Gazi, M. A ternary nanocomposites of graphene/TiO₂/polypyrrole for energy storage applications. *Fuller. Nanotub. Carbon Nanostructures* **2018**, *26*, 631–642. [[CrossRef](#)]
23. Benmoussa, D.; Molnar, K.; Hannache, H.; Cherkaoui, O. Development of thermo-regulating fabric using microcapsules of phase change material. *Mol. Cryst. Liq. Cryst.* **2015**, *627*, 163–169. [[CrossRef](#)]
24. Sobolciak, P.; Karkri, M.; Al-Maadeed, M.; Krupa, I. Thermal characterization of phase change materials based on linear low-density polyethylene, paraffin wax and expanded graphite. *Renew. Energy* **2016**, *88*, 372–382. [[CrossRef](#)]
25. Liu, S.; Han, L.; Xie, S.; Jia, Y.; Sun, J.; Jing, Y.; Zhang, Q. A novel medium-temperature form-stable phase change material based on dicarboxylic acid eutectic mixture/expanded graphite composites. *Sol. Energy* **2017**, *143*, 22–30. [[CrossRef](#)]
26. Ramakrishnan, S.; Wang, X.; Sanjayan, J. Thermal enhancement of paraffin/hydrophobic expanded perlite granular phase change composite using graphene nanoplatelets. *Energy Build.* **2018**, *169*, 206–215. [[CrossRef](#)]
27. Sari, A. Fabrication and thermal characterization of kaolin-based composite phase change materials for latent heat storage in buildings. *Energy Build.* **2015**, *96*, 193–200. [[CrossRef](#)]
28. Liu, S.; Yang, H. Composite of coal-series kaolinite and capric-lauric acid as form-stable phase-change material. *Energy Technol.* **2015**, *3*, 77–83. [[CrossRef](#)]
29. Jeong, S.; Jeon, J.; Chung, O.; Kim, S.; Kim, S. Evaluation of PCM/diatomite composites using exfoliated graphite nanoplatelets (xGnP) to improve thermal properties. *J. Therm. Anal. Calorim.* **2013**, *114*, 689–698. [[CrossRef](#)]
30. Liu, Z.; Hu, D.; Lv, H.; Zhang, Y.; Wu, F.; Shen, D.; Fu, P. Mixed mill-heating fabrication and thermal energy storage of diatomite/paraffin phase change composite incorporated gypsum-based materials. *Appl. Therm. Eng.* **2017**, *118*, 703–713. [[CrossRef](#)]
31. Karaipekli, A.; Sari, A. Preparation, thermal properties and thermal reliability of eutectic mixtures of fatty acids/expanded vermiculite as novel form-stable composites for energy storage. *J. Ind. Eng. Chem.* **2010**, *16*, 767–773. [[CrossRef](#)]
32. Ramakrishnan, S.; Wang, X.; Sanjayan, J.; Wilson, J. Assessing the feasibility of integrating form-stable phase change material composites with cementitious composites and prevention of pcm leakage. *Mater. Lett.* **2017**, *192*, 88–91. [[CrossRef](#)]
33. Dong, Z.; Meizhu, C.; Quantao, L.; Jiuming, W.; Jinxuan, H. Preparation and thermal properties of molecular-bridged expanded graphite/polyethylene glycol composite phase change materials for building energy conservation. *Materials* **2018**, *11*, 818.
34. Wang, F.; Xie, Z.; Liang, J.; Fang, B.; Piao, Y.; Hao, M.; Wang, Z. Tourmaline-Modified FeMnTiO_x Catalysts for Improved Low-Temperature NH₃-SCR Performance. *Environ. Sci. Technol.* **2019**, *53*, 6989–6996. [[CrossRef](#)]
35. Zhang, S.; Xue, X.; Liu, X.; Duan, P.; Yang, H.; Jiang, T.; Wang, D.; Liu, R. Current situation and comprehensive utilization of iron ore tailing resources. *J. Min. Sci.* **2006**, *42*, 403–408. [[CrossRef](#)]
36. Li, C.; Sun, H.; Yi, Z.; Li, L. Innovative methodology for comprehensive utilization of iron ore tailings: Part 2: The residues after iron recovery from iron ore tailings to prepare cementitious material. *J. Hazard. Mater.* **2010**, *174*, 78–83. [[CrossRef](#)]
37. Li, C.; Sun, H.; Bai, J.; Li, L. Innovative methodology for comprehensive utilization of iron ore tailings: Part 1. The recovery of iron from iron ore tailings using magnetic separation after magnetizing roasting. *J. Hazard. Mater.* **2010**, *174*, 71–77. [[CrossRef](#)]
38. Lv, P.; Liu, C.; Rao, Z. Review on clay mineral-based form-stable phase change materials: Preparation, characterization and applications. *Renew. Sustain. Energy Rev.* **2017**, *68*, 707–726. [[CrossRef](#)]
39. Song, X.; Cai, Y.; Huang, C.; Gu, Y.; Zhang, J.; Qiao, H.; Wei, Q. Cu nanoparticles improved thermal property of form-stable phase change materials made with carbon nanofibers and LA-MA-SA eutectic mixture. *J. Nanosci. Nanotechnol.* **2018**, *18*, 2723–2731. [[CrossRef](#)]
40. Han, J.; Liu, S. Myristic acid-hybridized diatomite composite as a shape-stabilized phase change material for thermal energy storage. *RSC Adv.* **2017**, *7*, 22170–22177. [[CrossRef](#)]

41. Yang, Y.; Pang, Y.; Liu, Y.; Guo, H. Preparation and thermal properties of polyethylene glycol/expanded graphite as novel form-stable phase change material for indoor energy saving. *Mater. Lett.* **2018**, *216*, 220–223. [[CrossRef](#)]
42. Amin, M.; Putra, N.; Kosasih, E.; Prawiro, E.; AchmadLuanto, R.; Mahlia, T. Thermal properties of beeswax/graphene phase change material as energy storage for building applications. *Appl. Therm. Eng.* **2017**, *112*, 273–280. [[CrossRef](#)]
43. Li, M.; Guo, Q.; Nutt, S. Carbon nanotube/paraffin/montmorillonite composite phase change material for thermal energy storage. *Sol. Energy* **2017**, *146*, 1–7. [[CrossRef](#)] [[PubMed](#)]
44. Sari, A.; Bicer, A.; Al-Sulaiman, F.; Karaipekli, A.; Tyagi, V. Diatomite/CNTs/PEG composite PCMs with shape-stabilized and improved thermal conductivity: Preparation and thermal energy storage properties. *Energy Build.* **2018**, *164*, 166–175. [[CrossRef](#)]
45. Wen, R.; Zhang, X.; Huang, Z.; Fang, M.; Liu, Y.; Wu, X.; Min, X.; Gao, W.; Huang, S. Preparation and thermal properties of fatty acid/diatomite form-stable composite phase change material for thermal energy storage. *Sol. Energy Mater. Sol. Cells* **2018**, *178*, 273–279. [[CrossRef](#)]
46. Li, X.; Chen, H.; Liu, L.; Lu, Z.; Sanjayan, J.; Duan, W. Development of granular expanded perlite/paraffin phase change material composites and prevention of leakage. *Sol. Energy* **2016**, *137*, 179–188. [[CrossRef](#)]
47. Lv, P.; Liu, C.; Rao, Z. Experiment study on the thermal properties of paraffin/kaolin thermal energy storage form-stable phase change material. *Appl. Energy* **2016**, *182*, 475–487. [[CrossRef](#)]
48. Gu, X.; Peng Liu, P.; Liang Bian, L.; He, H. Enhanced thermal conductivity of palmitic acid/mullite phase change composite with graphite powder for thermal energy storage. *Renew. Energy* **2019**, *138*, 833–841. [[CrossRef](#)]
49. Gu, X.; Liu, P.; Liu, C.; Peng, L.; He, H. A novel form-stable phase change material of palmitic acid-carbonized pepper straw for thermal energy storage. *Mater. Lett.* **2019**, *248*, 12–15. [[CrossRef](#)]
50. Gu, X.; Liu, P.; Bian, L.; Peng, L.; Liu, Y.; He, H. Mullite stabilized palmitic acid as phase change materials for thermal energy storage. *Minerals* **2018**, *8*, 440. [[CrossRef](#)]
51. Sari, A.; Karaipekli, A. Thermal properties and thermal reliability of capric acid/expanded perlite composite for thermal energy storage. *Mater. Chem. Phys.* **2008**, *109*, 459–464. [[CrossRef](#)]
52. Mei, D.; Zhang, B.; Liu, R.; Zhang, Y.; Liu, J. Preparation of capric acid/halloysite nanotube composite as form-stable phase change material for thermal energy storage. *Sol. Energy Mater. Sol. Cells* **2011**, *95*, 2772–2777. [[CrossRef](#)]
53. Karaipekli, A.; Sari, A. Capric–myristic acid/vermiculite composite as form-stable phase change material for thermal energy storage. *Sol. Energy* **2009**, *83*, 323–332. [[CrossRef](#)]
54. Shilei, L.; Neng, Z.; Guohui, F. Eutectic mixtures of capric acid and lauric acid applied in building wallboards for heat energy storage. *Energy Build.* **2006**, *38*, 708–711. [[CrossRef](#)]
55. Feldman, D.; Banu, D.; Hawes, D. Development and application of organic phase change mixtures in thermal storage gypsum wallboard. *Sol. Energy Mater. Sol. Cells* **1995**, *36*, 147–157. [[CrossRef](#)]
56. Karaman, S.; Karaipekli, A.; Sari, A.; Bicer, A. Polyethylene glycol (PEG)/diatomite composite as a novel form-stable phase change material for thermal energy storage. *Sol. Energy Mater. Sol. Cells* **2011**, *95*, 1647–1653. [[CrossRef](#)]
57. Hawes, D.; Feldman, D.; Banu, D. Latent heat storage in building materials. *Energy Build.* **1993**, *20*, 77–86. [[CrossRef](#)]
58. Memon, S.; Liao, W.; Yang, S.; Cui, H.; Shah, S. Development of composite PCMs by incorporation of paraffin into various building materials. *Materials* **2015**, *8*, 499–518. [[CrossRef](#)]
59. Biçer, A.; Sari, A. New kinds of energy-storing building composite PCMs for thermal energy storage. *Energy Convers. Manag.* **2013**, *69*, 148–156. [[CrossRef](#)]
60. Sari, A.; Karaipekli, A.; Kaygusuz, K. Capric acid and myristic acid for latent heat thermal energy storage. *Energy Sources Part A* **2008**, *30*, 1498–1507. [[CrossRef](#)]
61. Feldman, D.; Banu, D. DSC analysis for the evaluation of an energy storing wallboard. *Thermochim. Acta* **1996**, *272*, 243–251. [[CrossRef](#)]

62. Fang, G.; Li, H.; Cao, L.; Shan, F. Preparation and thermal properties of form-stable palmitic acid/active aluminum oxide composites as phase change materials for latent heat storage. *Mater. Chem. Phys.* **2012**, *137*, 558–564. [[CrossRef](#)]
63. Liu, P.; Gu, X.; Bian, L.; Cheng, X.; Peng, L.; He, H. Thermal properties and enhanced thermal conductivity of capric acid/diatomite/carbon nanotube composites as form-stable phase change materials for thermal energy storage. *ACS Omega* **2019**, *4*, 2964–2972. [[CrossRef](#)]



© 2019 by the authors. Licensee MDPI, Basel, Switzerland. This article is an open access article distributed under the terms and conditions of the Creative Commons Attribution (CC BY) license (<http://creativecommons.org/licenses/by/4.0/>).